Chapter 6

Cherenkov Radiation

The topics of energy loss by charged particles and Cherenkov radiation, even if seemingly unrelated, are closely connected (together with the topic of transition radiation – but we will let that rest, as its application in particle physics experiments is very rare). Cherenkov radiation is known since 1934, when Cherenkov performed his experimental studies; the theoretical explanation was provided by Frank and Tamm in 1937. (The discovery of Cherenkov radiation came relatively late, due to the -misguided- idea that no particle would be able to travel faster than the velocity of light *in a macroscopic medium*, although the theory of special relativity deals with the velocity of light *in vacuo* only.)

In the following, we will not use the full theoretical framework starting from Maxwell's equation in a macroscopic medium. Good texts taking this as a starting point (all in the framework of *classical* electrodynamics – a quantum treatment yields almost exactly the same results) are that by Allison and Wright [1], as well as Chapter 13 of the book by Jackson [2] and the 1958 Nobel lectures by Cherenkov, Frank, and Tamm.

6.1 Physical Principle

A good way to see qualitatively under which circumstances Cherenkov radiation can be generated is the following. We start from the assumption that a photon (of energy $\hbar\omega$ and momentum $\hbar\mathbf{k}$) *is* in fact emitted by a relativistic charged particle. Conservation of four-momentum then requires that

$$\hbar(\omega^2/c^2 - k^2) = 2m\gamma(\omega - \beta ck\cos\theta), \tag{6.1}$$

where θ is the angle between the direction of the emitted photon and the direction of movement of the charged particle. Now we use the dispersion relation for a macroscopic medium of refractive index n,

$$\omega = ck/n,$$

and we consider the limit in which the photon energy is negligible compared to that of the charged particle. In that case, we must have

$$n\beta\cos\theta = 1. \tag{6.2}$$

Clearly, Cherenkov radiation can occur only if $\beta > 1/n$. The maximum emission angle is reached for a particle approaching infinite momentum, $\beta = 1$: $\cos\theta_{\max} = 1/n$. It has furthermore been verified that the polarization vector of the emitted photons lies in the plane spanned by the direction of the

photon and the charged particle (though in present-day applications, this polarization is practically never made use of).

(Another way to view the emission angle is by *Huijgens' construction* in the presence of a shock wave: a plane-wavefront can be constructed only for exactly this angle.)

Another important feature is the *radiated power*. Assuming that our particle's charge is equal to one, this is given by the *Frank-Tamm law*:

$$\frac{\mathrm{d}E}{\mathrm{d}x\mathrm{d}\omega} = \frac{\hbar\alpha}{c}\left(1 - \frac{1}{\beta^2 n^2}\right)\omega. \tag{6.3}$$

It is easy to convert this to an expression for the amount of photons generated:

$$\frac{\mathrm{d}N}{\mathrm{d}x\mathrm{d}\omega} = \frac{\alpha}{c}\left(1 - \frac{1}{\beta^2 n^2}\right) = \frac{\alpha}{c}\sin^2\theta(\omega).$$

Finally, this equation is often rewritten in terms of the photon's *energy* E_γ rather than its frequency; we then obtain for the *total* number of Cherenkov photons

$$N_\gamma = \frac{\alpha L}{\hbar c}\int_{\beta n(E_\gamma)>1} \sin^2\theta(E_\gamma)\mathrm{d}E_\gamma \approx 370(\mathrm{eV}\cdot\mathrm{cm})^{-1}\int_{\beta n(E_\gamma)>1} \sin^2\theta(E_\gamma)\mathrm{d}E_\gamma$$

Merely from the presence of the factor α in this equation, one can expect the number of photons generated by Cherenkov radiation to be small compared to other radiation mechanisms, *e.g.* scintillation. Even when multiplying the prefactor 370 in the last equation with a large length, typical numbers of detected Cherenkov photons are several tens to several hundreds, due to the suppression by the factor $\sin^2\theta$ as well as the instrumental limitations given further down. Indeed, this feature contributed to the "late" discovery of Cherenkov radiation.

Finally, it is worth noticing at this point that no relaxation phenomena are involved in the emission of Cherenkov radiation. This implies that this radiation takes place *instantly*.

6.1.1 Behaviour of the refractive index

To go beyond the general formula of Eqn. 6.3, we have to know the expression for the refractive index as a function of frequency. In general, this is related to the relative dielectric constant and magnetic permeability:

$$n^2(\omega) = \varepsilon(\omega)\mu(\omega);$$

In the remainder of the Chapter, we will be dealing with dielectrics only, *i.e.* we can set $\mu(\omega)$ equal to one.

It is in principle possible to derive the full dependence of the relative dielectric constant on frequency, through the following steps:

1. It has to be kept in mind that ε is an intrinsically *complex* variable, with the imaginary part representing absorption (it is this part which makes the connection with the energy loss due to ionization and excitation, see *e.g.* Jackson, Chapter 13) and the real part representing refraction. Therefore, the imaginary part $\Im(\varepsilon)$ can in principle be derived from photoabsorption measurements. In practice, the photoabsorption cross-section is non-zero only above a certain threshold. To simplify matters, we can represent this threshold by a delta function:

$$\Im(\varepsilon(\omega)) = \frac{\pi K}{2\omega_0}\delta(\omega - \omega_0).$$

2. If the imaginary part of ε is known, its real part can be computed through the use of the *Kramers-Kronig* relation:
$$\Re(\varepsilon(\omega)) = 1 + \frac{2}{\pi} P \int_0^\infty \frac{\omega' \Im(\varepsilon(\omega'))}{\omega'^2 - \omega^2} \mathrm{d}\omega'.$$
In the above simplified case, this relation simplifies to
$$\Re(\varepsilon(\omega)) = 1 + \frac{K}{\omega_0^2 - \omega^2}.$$
The fact that in reality, the imaginary part is not really a delta function can be taken into account by replacing the 1 in the above equation by a constant ε_0.
Qualitatively, the behaviour of $\varepsilon(\omega)$ is generally as follows: the cutoff frequency ω_0 is located in the UV part of the spectrum. In the visible region therefore, ε varies fairly smoothly as a function of ω. Cherenkov radiation then occurs only between near-IR and near-UV frequencies.

3. When dealing with gases, we can be slightly more specific, as in this case the dependence on the density can be taken into account explicitly. We use the *Lorentz-Lorenz* relation (see *e.g.* Jackson, Chapter 4)
$$\frac{n^2 - 1}{n^2 + 2} \frac{m}{\rho} = R', \tag{6.4}$$
where m is the molecular mass, ρ is the gas density, and R' is a constant. We then use the fact that $n \approx 1$ to simplify Eqn. 6.4 to
$$n - 1 \approx \frac{3}{2} \frac{R'}{m} \rho.$$
Now, for an ideal gas we have $P = \rho RT/m$. Therefore, even without the explicit knowledge of the quantity R' we know that the dependence on temperature and pressure must be given by
$$n - 1 \approx (n_0 - 1) \frac{(P/T)}{(P_0/T_0)}.$$

6.2 Cherenkov Counters

The use of Cherenkov radiation in particle physics experiments is solely for the purpose of particle identification: since a measurement of the Cherenkov angle θ would provide a measurement of β, the corresponding uncertainty on the particle *momentum* would scale as
$$\frac{\Delta p}{p} = \gamma^2 \frac{\Delta \beta}{\beta},$$
implying that for large momenta, $\Delta p/p \sim p^2$, *i.e.* worse than for tracking detectors.

In the following we describe the most often used applications.

6.2.1 Threshold Cherenkov counters

As its name indicates, the threshold Cherenkov counter's primary use is to determine whether a particle's velocity exceeds a given threshold. This is most useful in beam lines, in which the particle momentum is fixed. The Cherenkov counter in this case is typically a simple gas-filled volume, as depicted in Figure 6.1. A tilted spherical mirror is used to focus the emitted Cherenkov photons onto the

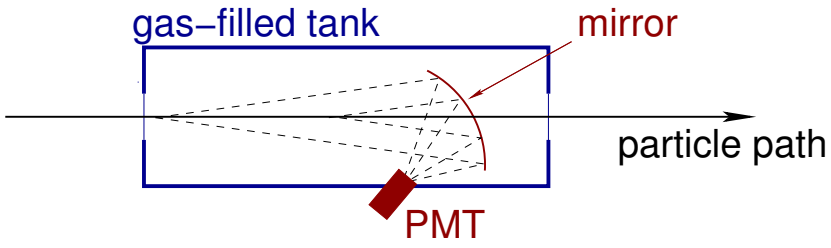

Figure 6.1: Threshold Cherenkov counter

photocathode of a PMT. The tilt is necessary as otherwise the PMT would be right in the beam line. The mirror needs to be thin to minimize multiple Coulomb scattering; the same holds for the entrance and exit windows of the radiator volume. The threshold setting obviously depends on what particles need to be distinguished from each other (often pions from kaons), and is most easily changed by varying the pressure in the vessel.

Further optimization is obtained by the usual desire to maximize the number of *detected* photoelectrons. This is given by

$$N_\gamma \approx 370(\text{eV}\cdot\text{cm})^{-1}\int_{\beta n(E_\gamma)>1} Q(E_\gamma)T(E_\gamma)R(E_\gamma)\sin^2\theta(E_\gamma)\mathrm{d}E_\gamma \tag{6.5}$$

where:

- R is the reflection coefficient of the mirror: different coatings can have a significantly different wavelength dependence. Normal mirrors typically use Ag, which has a high reflection coefficient (above 90%) for wavelengths above 500 nm. For an increased sensitivity to shorter wavelengths, which is typically desired in connection with the quantum efficiency of often-used photocathodes (see below), Al or MgF_2 can be used;

- T is the transmission coefficient of the entrance window of the PMT: as for the reflectivity of the mirror, a proper choice of material needs to be made. Many PMTs come with borosilicate glass (a mixture of essentially SiO_2 and B_2O_3; Pyrex is a well-known example) windows, which becomes transmissive for wavelengths above 350-400 nm. For improved UV and/or blue sensitivity, fused silica or quartz can be used. Figure 6.2 shows a comparison of several materials.

- Q is the PMT photocathode's quantum efficiency. For many photocathodes the maximum quantum efficiency is reached for relatively short wavelengths, as shown *e.g.* in Figure 6.3. Unless one resorts to using semiconducting materials, there is typically not very much that can be done about this.

Often, over the wavelength range that can be covered by a photodetector system, the dispersion is low and the Cherenkov angle can be considered constant. In that case, Eqn. 6.5 can be conveniently separated into a term N_0 characterizing the experimental setup, and the term $\sin^2\theta$ purely due to the Frank-Tamm law:

$$N_\gamma \approx N_0\sin^2\theta, \quad N_0 = 370(\text{eV}\cdot\text{cm})^{-1}\int Q(E_\gamma)T(E_\gamma)R(E_\gamma)\mathrm{d}E_\gamma$$

Note that in principle, even with a simple device such as the threshold Cherenkov counter one could do more than just distinguish whether a particle is above or below the threshold for Cherenkov

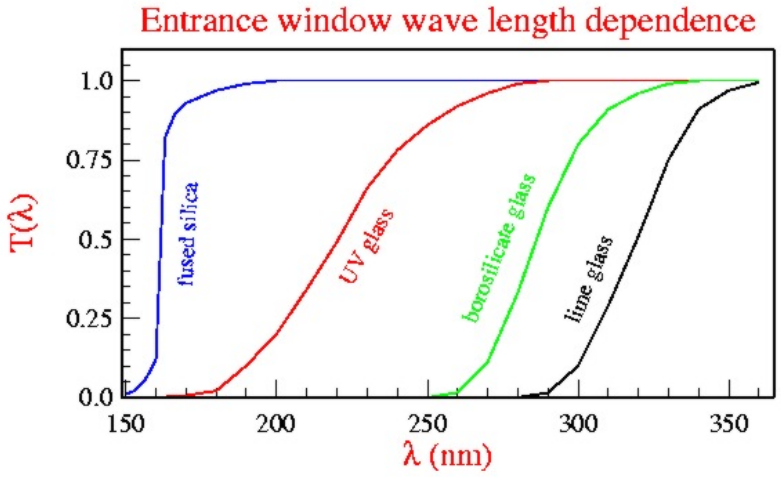

Figure 6.2: Transmission for several often-used photomultiplier entrance windows

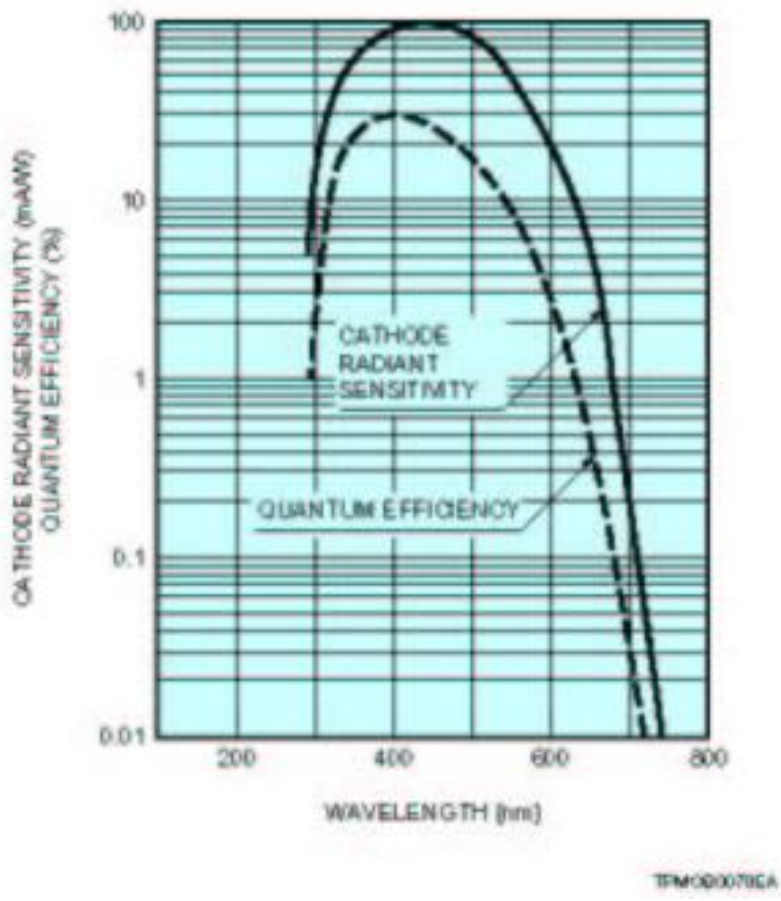

Figure 6.3: Quantum efficiency for a bialkali photocathode (from Hamamatsu)

radiation: the *number* of radiated photons is also an indication for how far above the threshold a particle sits. Therefore, if one could properly count the number of generated photons, it would be possible to distinguish different particles above threshold. However, the limited capabilities of a PMT make this impossible, and another sort of (photon counting) photodetector would have to be resorted to.

6.2.2 Ring Imaging Cherenkov counters

The usefulness of threshold Cherenkov counters is somewhat limited by the fact that they must a be optimized for a limited momentum region. In a collider detector, one would like to have particle identification capabilities over a large momentum range. This is offered by the Ring Imaging CHerenkov counter or RICH: rather than merely distinguishing whether a particle's velocity exceeds the Cherenkov radiation threshold, this device attempts to reconstruct explicitly the Cherenkov *angle* under which the photons are emitted.

The RICH detector was invented by J. Séguinot and T. Ypsilantis in 1977 [3]. Its principle of operation is shown in Figure 6.4 (this Figure can be thought of as the axial view of a collider detector). In this figure, charged particles radiate Cherenkov photons in the medium between radii $r = R/2$ and

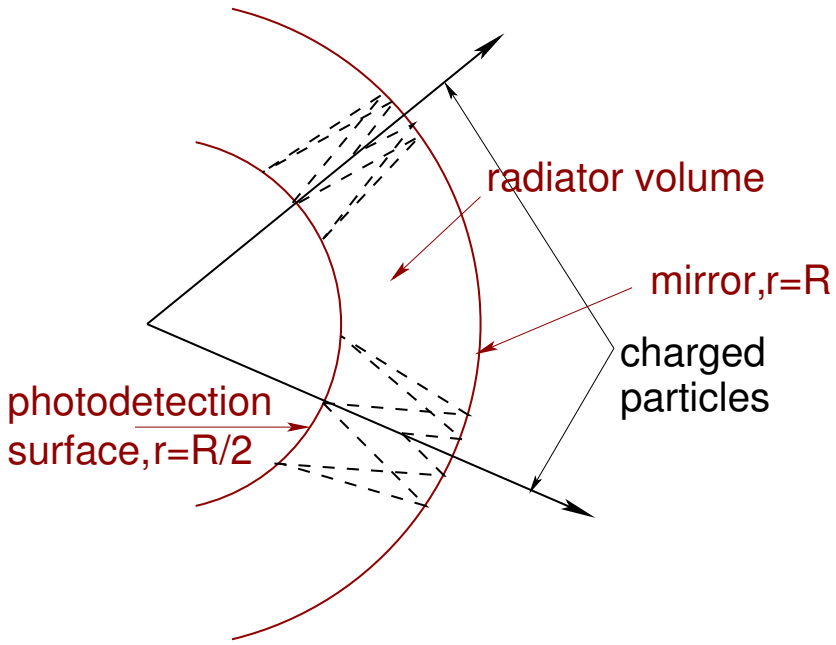

Figure 6.4: Operating principle of the RICH detector

$r = R$. From a simple optics argument it can be seen that the emitted photons will be focused onto the circle with radius $r = R/2$:

1. from the standard reconstruction of focal planes

$$\frac{1}{x_1} + \frac{1}{x_2} = \frac{1}{f},$$

with f the focal length of the lens (or in this case, mirror), and with $x_1^{-1} = 0$ for parallel incoming rays, one has $x_2 = f$;

2. from the fact that for this spherical mirror, photons emitted from $r = 0$ would be refocused at $r = 0$, corresponding to $x_1 = x_2 = 2f = R$, one has $f = R/2$. Therefore, the circle with radius $r = R - f = R/2$ becomes the focal "plane" for photons emitted in parallel.

Note that this focusing is perfect only for a parabolic mirror, on axis; but for large radii, spherical mirrors are a very good approximation.

The technical challenge for a practical RICH detector is to design the focal plane in such a way that the position of incident photons can be reconstructed accurately. The two applications of RICH detectors described in the following differ greatly in this respect.

DELPHI

DELPHI was one of the first "major" collider experiments (after the Mark I and Mark II e^+e^- experiments at lower energies at SLAC) to use RICH techniques for the identification of charged hadrons. Given the relatively large bunch spacing at LEP (45 μs), it could afford to transport all of its detected photoelectrons to the end of the detector and there read them out using a MWPC. A sketch of the DELPHI barrel RICH detector's operating principle is shown in Figure 6.5. Its resulting design is

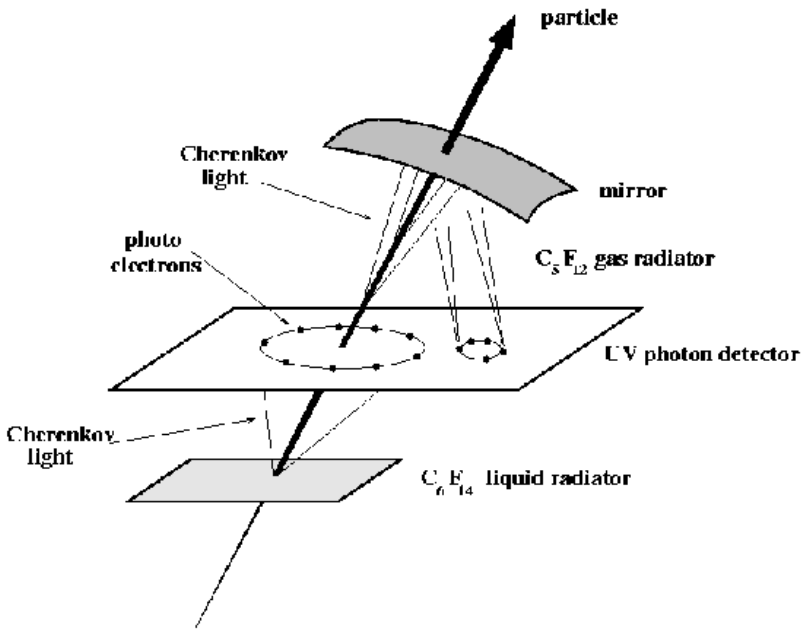

Figure 6.5: Particle identification using two radiators in the DELPHI experiment's barrel RICH detector. Courtesy CERN

shown in Figure 6.6.

This detector consists in fact of *two* radiator volumes:

- one consisting of 1 cm of C_6F_{14} liquid, with refractive index $n = 1.28$;
- and one consisting of 40 cm of C_5F_{12} gas (the whole detector was operated at a temperature of 40 °C, to be above the boiling point of C_5F_{12}, 28 °C), with refractive index $n = 1.0018$.

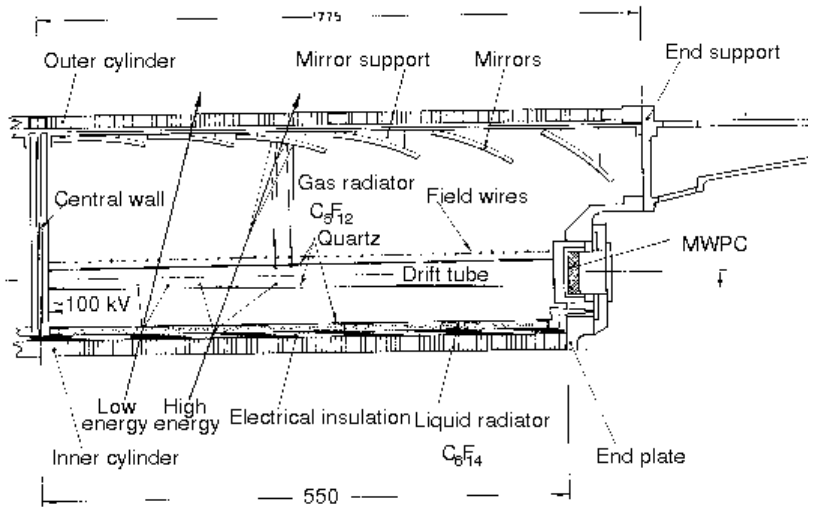

Figure 6.6: Design of the DELPHI experiment's barrel RICH detector. Courtesy CERN

The use of two radiators allows to obtain a good particle identification at low as well as high momenta: using only the gaseous radiator would lead to many low-momentum π/K being below the Cherenkov radiation threshold; and using only the liquid radiator would lead to a strongly reduced π/K separation for high momenta.

Note, furthermore, that no focusing is applied to the liquid radiator. This is sufficiently thin (with its 1 cm) that photons emitted in parallel will not end up in significantly different positions on the photodetector: this setup is often called *proximity focusing*. This is in contrast with the gaseous radiator, where a thickness of 40 cm clearly necessitates focusing mirrors.

The other noteworthy feature is that the photodetector used in this case is not a PMT or other solid-state device, but a photosensitive gas called tetrakis (dimethylamine) ethylene or TMAE, admixed to a drift gas consisting of a methane-ethane mixture. TMAE is sensitive to UV photons, for photon energies above 5.4 eV. Note that this also requires housing the drift tube, in which this gas is located, in a material that has a good transparency for UV light (quartz).

The photoelectrons then drift towards the end plate: like in a TPC, this drift is along the magnetic field, thereby ensuring low diffusion.

Cherenkov angular measurements performed using this detector, both for the liquid (top) and gaseous radiator (bottom) are shown in Figure 6.7. (Note that in practice, it is often possible to distinguish which photons are to be associated with which radiator. This is because one can assume the charged particle's momentum to be known *a priori*, from tracking measurements. Moreover, in this case, the Cherenkov angles for the gaseous and liquid radiators differ by an order of magnitude.) Notice that for the very highest momenta, the π/K separation again becomes worse. However, it has to be kept in mind that the LEP collider operated only at centre-of-mass energies up to about 200 GeV, and most of its precision data (where π/K separation is most useful) were taken at the Z resonance. So the track momenta involved are in general not very high.

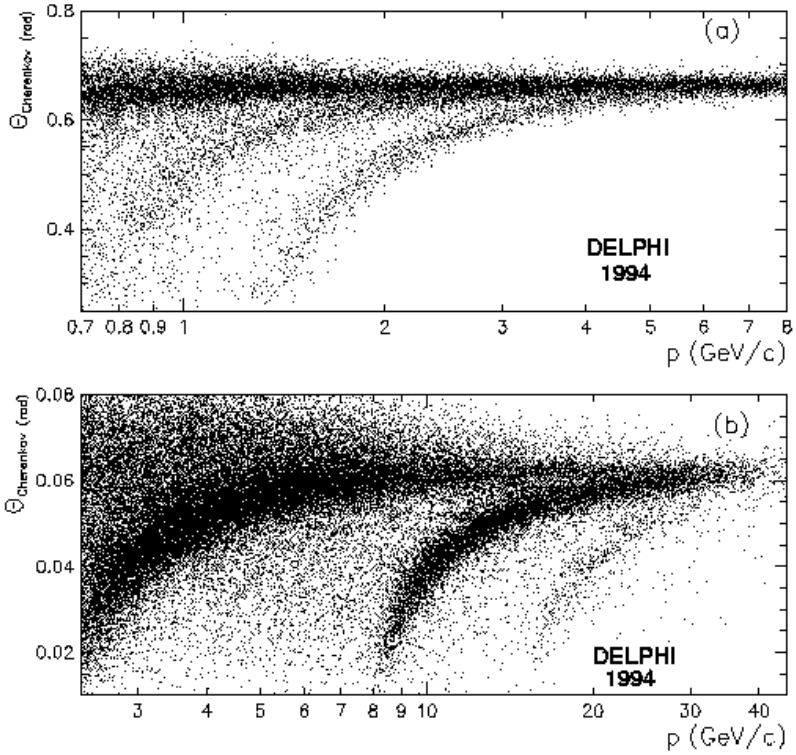

Figure 6.7: Performance of the DELPHI barrel RICH detector. Courtesy CERN

LHCb

The LHCb experiment is a significantly different detector. As its name indicates, it is an experiment at the LHC, which means that the bunch spacing of 25 ns is much too short to use a drift chamber. On the other hand, although LHCb is located at a collider, it is built much like the spectrometer for a fixed-target experiment, as shown in Figure 6.8.

The reason for the particular shape is related to the physics goal of the experiment: it is intended to perform precision studies of various B meson decay modes, and in particular of CP violation. At the 14 TeV centre-of-mass energy of p-p collisions in the LHC, the vast majority of the B mesons are produced in the far forward direction. Therefore, a single spectrometer (of sufficiently large aperture) suffices to obtain a large acceptance for such events.

In this spectrometer structure, the space constraints are much less severe than in the case of the DELPHI experiment: it is much easier to place the readout electronics of the subdetectors at the perimeter of these subdetectors themselves. How this is done in the case of the RICH detectors (the experiment has two of them) is shown in Figure 6.9. The reason for using two RICH detectors is the fact that the momentum range that needs to be covered for π/K separation is much larger than in the case of LEP, due to the LHC being a hadron collider. Given that the *transverse* momenta do not vary greatly even when the longitudinal ones do, there is a general anti-correlation between the angles with the beam line under which particles are emitted and their momenta. Therefore, using one detector optimized for high momenta at low angles, and using one optimized for lower momenta at higher angles is a good way to obtain a good overall performance. The first RICH detector even features two radiators: one of them, Silica aerogel, is a colloidal form of quartz (*i.e.* a mixture of

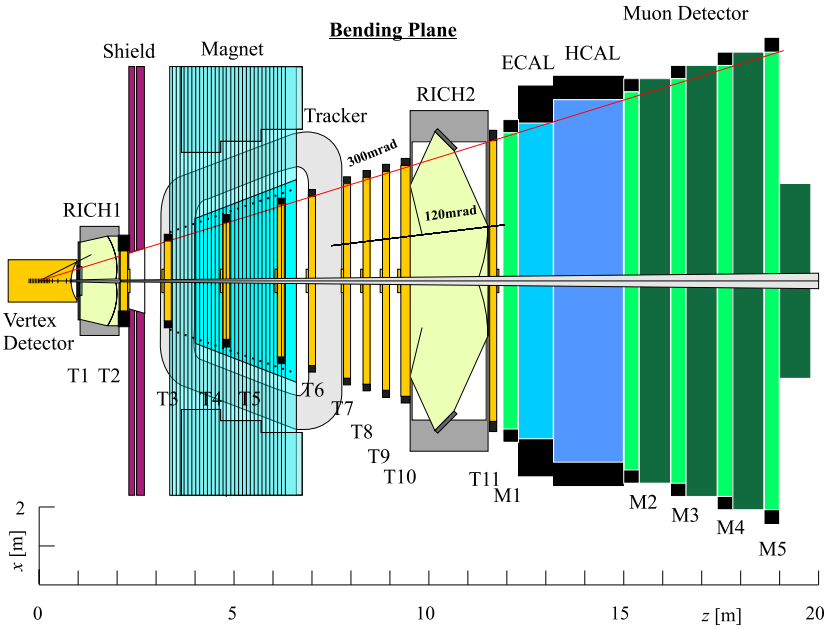

Figure 6.8: Layout of the LHCb experiment (horizontal projection). Courtesy CERN

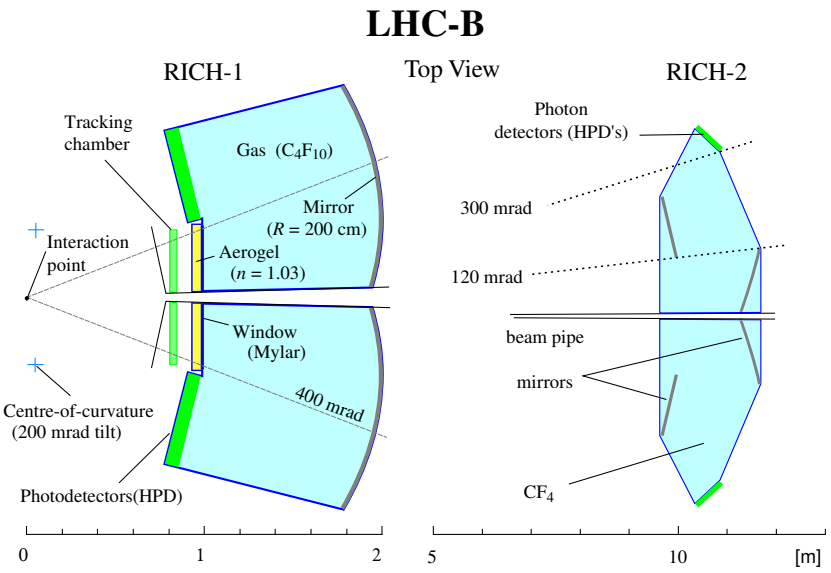

Figure 6.9: Design of the RICH detectors of the LHCb experiment. Courtesy CERN

SiO_2 and H_2O molecules) that microscopically looks much like soap bubbles. The advent of these arogels (they are difficult to produce), with refractive indices filling a gap between the highest indices for gaseous media and the lowest indices for liquids, was an important ingredient in the usefulness of RICH detectors.

Another significant difference with respect to the LEP case is the fact that it is not possible to use drift chambers as photodetectors, and solid state photodetectors have to be resorted to. Simple PMTs will not do, however, because they do not allow reconstruction of Cherenkov angles with the required accuracy: to do so requires segmenting the photodetector plane in elements of roughly 6 mm^2!

In principle, PMTs with segmented anodes can now be bought (and indeed, this has long been a fall-back option for the LHCb experiment). However, another option was finally adopted: the Hybrid PhotoDiode or HPD. In its simplest form, the operating principle of an HPD is shown in Figure 6.10. As can be seen, the HPD looks like a regular PMT in the sense that it employs a "standard" (bialkali

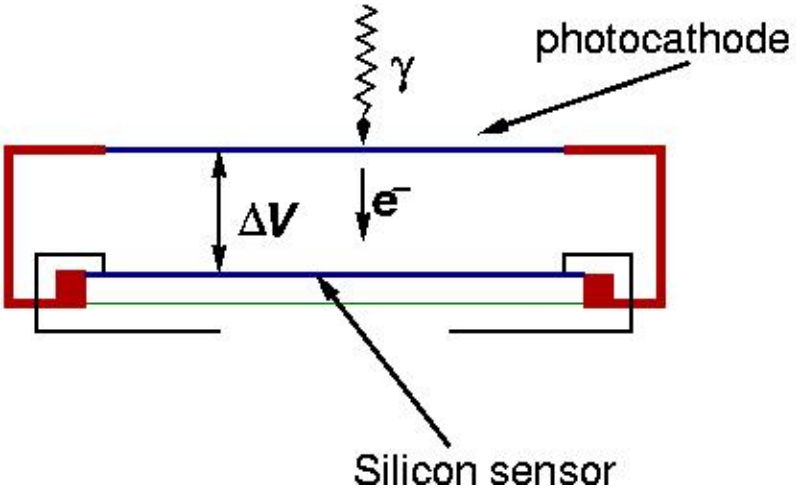

Figure 6.10: Operating principle of the HPD

or multi-alkali) photocathode (hence its name!). However, the dynode amplification stage is replaced with a simple photoelectron acceleration in an electric field. The photoelectron then impinges on a silicon sensor, where it is stopped and deposits all its energy in the form of e-h pairs. This is shown in more detail in Figure 6.11. This sort of detector offers several advantages over a PMT:

- like the VLPC, it allows *photon counting*: the photoelectron deposits all its energy (apart from a small amount lost in the "dead" Al layer) in the sensor's depletion region, and therefore again Poisson statistics with a mean of several thousands applies (depending on the voltage setting);
- the signal linearity is very good (once the incident electrons' energy is high enough to traverse the n^+ layer without losing too much energy; in this layer, no useful signal is generated), being determined purely by the applied high voltage;
- and the sensor can be *segmented*. If the distance between photocathode and anode is kept small, this leads to a good correlation between the position on the silicon sensor and the impact point of the Cherenkov photon – even in strong magnetic fields.

Figure 6.12 shows the photon counting capabilities and the linearity of the HPD.

Unfortunately, it turns out that quite a bit of space is required to house electronics in the HPD volume, required to multiplex (serialize) the readout of many silicon channels. For the purpose of the

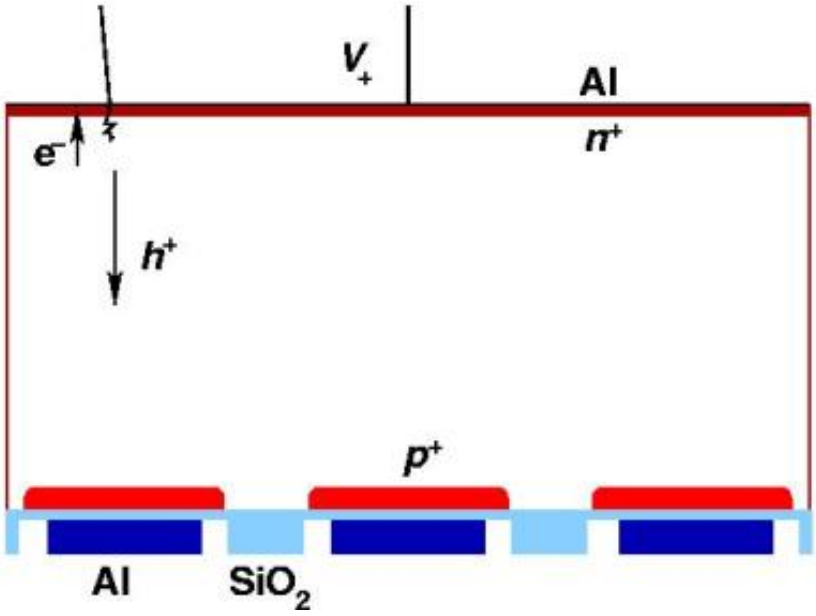

Figure 6.11: Photoelectron impinging on an HPD sensor

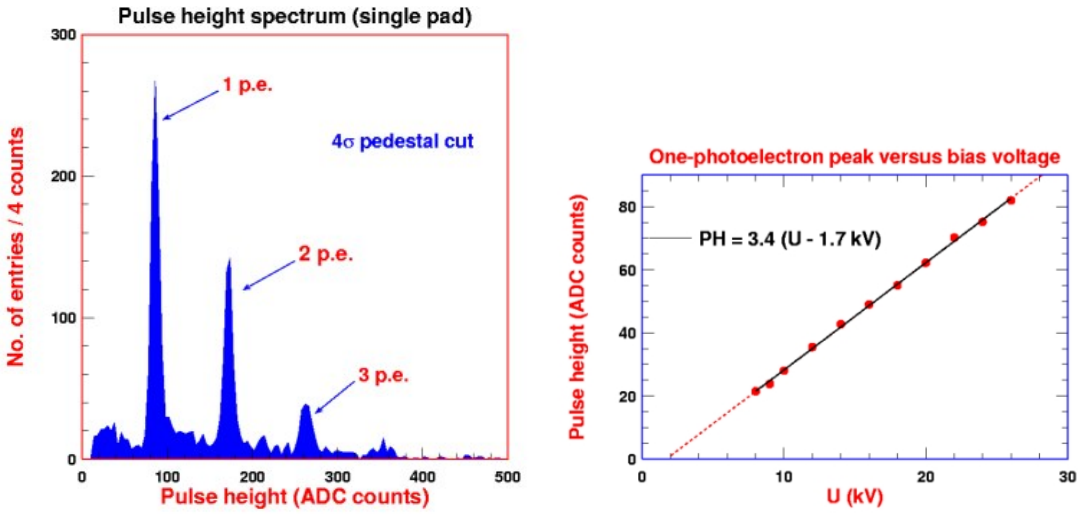

Figure 6.12: Pulse height spectrum and position of the first peak as a function of applied voltage

LHCb detector, this would have led to too large a loss of Cherenkov photons. Therefore, together with industry (Delft Electronics Products, now merged with PMT producer Photonis), a project was started to produce *focusing* HPDs, which reduce the "image" of the photocathode by a factor of about four (onto sensor pixels of about $500\mu\text{m} \times 500\mu\text{m}$, so that there remains enough space to house electronics. This imaging requires a careful shaping of the electrical field, necessitating long drift distances; and as a consequence, large distortions of the image occur for relatively low magnetic field (several tens of Gauss). The devices therefore need to be properly shielded. Figure 6.13 shows the cross-focusing electric field used in the resulting devices.

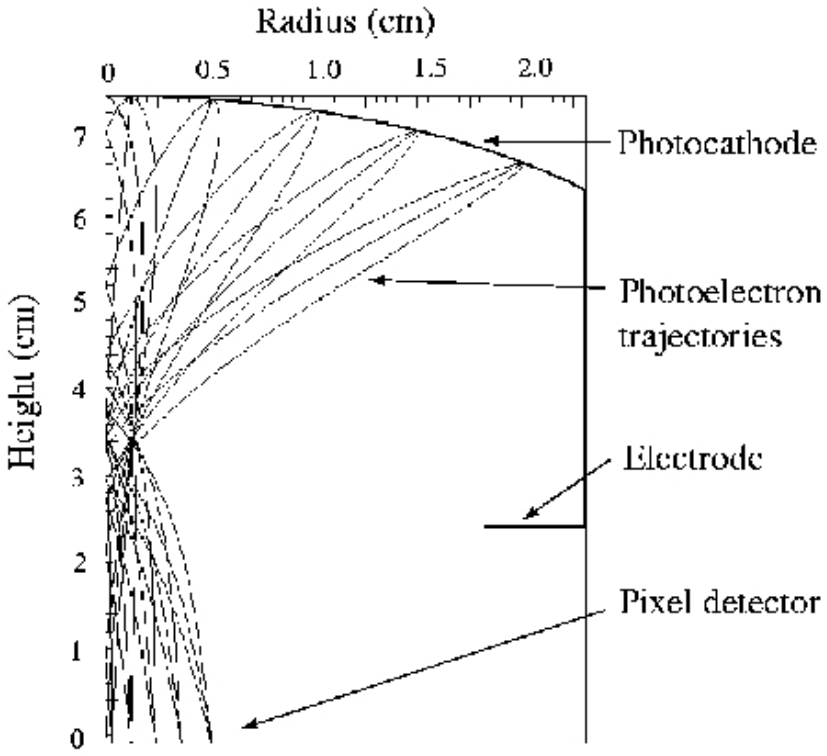

Figure 6.13: Cross-focusing optics of the LHCb pixel HPD. One should imagine this image mirrored along the vertical axis to obtain the actual trajectories. Courtesy CERN

The expected performance of this detector is very good: even in a situation where a complicated pattern recognition needs to be done, as shown in Figure 6.14, it is expected that π/K separation can be done with very good efficiency for momenta between 3 GeV and 75 GeV.

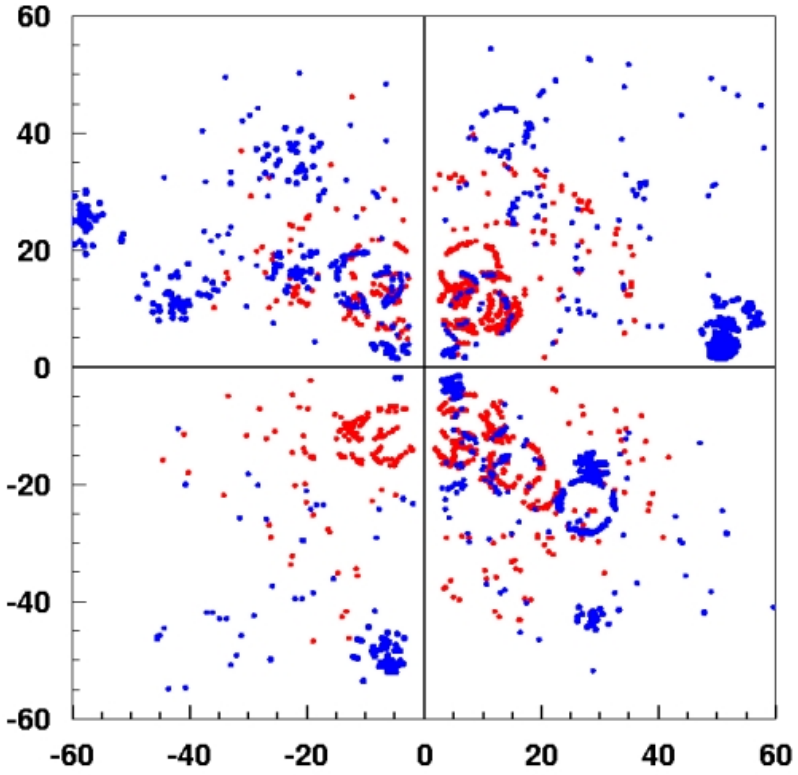

Figure 6.14: One (simulated) event as seen by the photodetectors of the first RICH detector of the LHCb experiment. The red dots represent photoelectrons due to Cherenkov photons generated in the RICH radiators; the blue dots represent background hits.

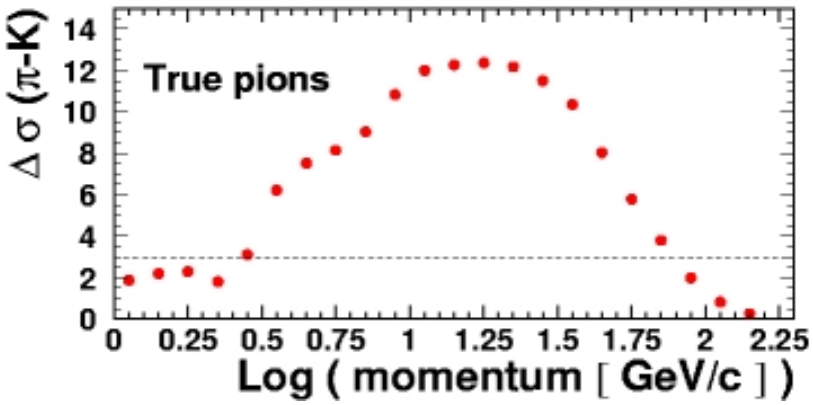

Figure 6.15: Expected π/K seperation as a function of momentum in the LHCb RICH detectors

Bibliography

[1] W.W.M. Allison and P.R.S. Wright, *The Physics of Charged Particle Identification:* dE/dx, *Cherenkov and Transition Radiation*, Addison-Wesley, 1987, ISBN 0-201-11487-9

[2] J.D. Jackson, Classical Electrodynamics, (Wiley, 1975), ISBN 0-471-43132-X

[3] J. Séguinot and T. Ypsilantis, Nucl. Instr. Meth. **142** (1977) 377